Available online at www.sciencedirect.com
ScienceDirect
International Journal of Impact Engineering 35 (2008) 829–844
INTERNATIONAL JOURNAL OF IMPACT ENGINEERING
www.elsevier.com/locate/ijimpeng

# The dynamic response of end-clamped sandwich beams with a Y-frame or corrugated core

V. Rubino, V.S. Deshpande, N.A. Fleck*

*Engineering Department, Cambridge University, Trumpington Street, Cambridge CB2 1PZ, UK*

Received 13 July 2007; received in revised form 29 October 2007; accepted 29 October 2007
Available online 15 December 2007

**Abstract**

The dynamic response of end-clamped monolithic beams and sandwich beams has been measured by loading the beams at mid-span using metal foam projectiles. The AISI 304 stainless-steel sandwich beams comprise two identical face sheets and either prismatic Y-frame or corrugated cores. The resistance to shock loading is quantified by the permanent transverse deflection at mid-span of the beams as a function of projectile momentum. The prismatic cores are aligned either longitudinally along the beam length or transversely. It is found that the sandwich beams with a longitudinal core orientation have a higher shock resistance than the monolithic beams of equal mass. In contrast, the performance of the sandwich beams with a transverse core orientation is very similar to that of the monolithic beams. Three-dimensional finite element (FE) simulations are in good agreement with the measured responses. The FE calculations indicate that strain concentrations in the sandwich beams occur at joints within the cores and between the core and face sheets; the level of maximum strain is similar for the Y-frame and corrugated core beams for a given value of projectile momentum. The experimental and FE results taken together reveal that Y-frame and corrugated core sandwich beams of equal mass have similar dynamic performances in terms of rear-face deflection, degree of core compression and level of strain within the beam.


*Keywords:* Sandwich beams; Dynamic response; FE simulations; Lattice materials

## 1. Introduction

Clamped sandwich beams are representative of sub-structures used in land-based and sea-based vehicles. These commercial and military vehicles are potentially subjected to dynamic loading above the quasi-static collapse strength. The response of monolithic beams and plates to shock-type loading has been extensively investigated. For example, Wang and Hopkins [1] and Symonds [2] have analysed the impulsive response of clamped circular plates and beams, respectively. However, their analyses were restricted to small deflections and linear bending kinematics. By direct application of the principle of virtual work for an assumed deformation mode, Jones [3] presented an approximate solution for simply supported circular monolithic plates undergoing finite deflections. Recently, Fleck and Deshpande [4] proposed an analytical model for the response of clamped sandwich beams to shock loadings including the effects of fluid–structure interaction: these analytical predictions are in close agreement with the finite element (FE) calculations of Xue and Hutchinson [5].

Over the past decade there have been substantial changes in ship design, see for example the review by Paik [6]. In the current study, we measure and analyse the dynamic performance of sandwich beams with a Y-frame sandwich core, as proposed by Schelde Shipbuilding[1] and as sketched in Fig. 1a. Full-scale ship collision trials reveal that the Y-frame design is more resistant to tearing than conventional monolithic designs, see Wevers and Vredeveldt [7] and Ludolphy [8]. Likewise, the FE simulations by Konter [9] suggest that the Y-frame confers improved perforation resistance. Naar et al. [10] have argued in broad terms that the ability of the bending-governed Y-frame topology to spread the impact load over a wide area, combined with the

*Corresponding author. Tel.: +44 1223 748240; fax: +44 1223 332662.
*E-mail address:* naf1@eng.cam.ac.uk (N.A. Fleck).

[1]Royal Schelde, P.O. Box 16, 4380 AA Vlissingen, The Netherlands.

0734-743X/$ - see front matter 
doi:10.1016/j.ijimpeng.2007.10.006

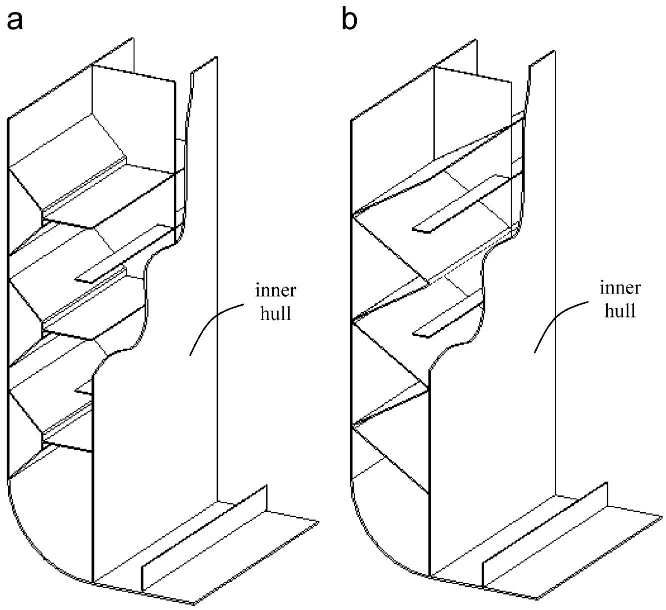


Fig. 1. Sketch of the (a) Y-frame and (b) corrugated sandwich cores as used in ship hull construction. The core is sandwiched between the inner and outer hulls of the ship.

in-plane high stretching resistance of the Y-frame, gives the enhanced performance of the Y-frame sandwich construction over conventional single and double hull designs. Similar to the Y-frame, the folded plate or corrugated sandwich core (Fig. 1b) has a prismatic topology and is considered as an alternative to the Y-frame design. The main aim of this study is to contrast the dynamic performances of sandwich beams with Y-frame and corrugated cores.

Pedersen et al. [11] and Rubino et al. [12,13] have investigated the *quasi-static* properties of Y-frame sandwich core structures while Côté et al. [14] studied the quasi-static response of the corrugated sandwich core. These studies reveal that the perfect corrugated core, absent geometrical imperfections and subjected to uniform macroscopic loading, is significantly stronger than the Y-core: the corrugated core deforms by plastic stretching of its struts, while the Y-core deforms by plastic bending. Geometrical imperfections and/or non-uniform loading (such as indentation loading) induce bending within the struts of the corrugated core and reduce its strength to approximately that of the Y-core.

Tilbrook et al. [15] have recently conducted a combined experimental and numerical investigation of the dynamic compressive response of the Y-frame and corrugated cores. They noted that the dynamic responses of the cores were dictated by (i) inertial stabilisation of the webs against buckling and (ii) plastic shock wave effects. Inertial stabilisation of the webs against buckling is the dominant dynamic strengthening mechanism at low velocities. At higher impact velocities, a plastic shock elevates the front face stresses above the level of rear face stress. To date, there have been little (or no) experimental data published on the dynamic response of Y-frame and corrugated sandwich core sandwich beams.

Only limited experimental data exist for blast loaded plates, with critical studies performed by Nurick and co-workers [16,17] who investigated the spatially uniform and localised blast response of square monolithic plates. By contrast, Radford et al. [18] have developed an experimental technique to subject structures to high-intensity pressure pulses using metal foam projectiles. The applied pressure versus time pulse mimics shock loading in air and in water, with peak pressures on the order of 100 MPa and loading times of approximately 100 μs. This laboratory method has been employed by Radford et al. [19] and Rathbun et al. [20] to investigate the dynamic response of clamped sandwich beams with metal foam and lattice cores. In the current study, we shall employ this experimental technique to explore the shock resistance of clamped sandwich beams with Y-frame and corrugated sandwich cores. The outline of the paper is as follows. First, the manufacturing route of the sandwich beams is detailed and the experimental protocol is described for loading the beams at mid-span by metal foam projectiles. The experimental results are discussed for two orientations of the core in the sandwich beams and for monolithic beams, and are then compared with FE predictions.

## 2. Experimental investigation

Metal foam projectiles were used to load dynamically clamped sandwich beams. The beams were made from AISI 304 stainless steel, and comprised two identical face sheets and either a Y-frame core or a corrugated core. The loading arrangement is sketched in Fig. 2a for the case of the Y-frame sandwich beam. The primary objectives of the experimental investigation are

(i) To compare the dynamic resistance of the sandwich beams with monolithic beams of equal areal mass, and made from the same material.
(ii) To contrast the dynamic strengths of sandwich beams made from a corrugated core and a Y-frame core.
(iii) To determine the accuracy of three-dimensional FE calculations in predicting the dynamic response and the onset of failure in the sandwich beams.

### 2.1. Specimen configuration and manufacture

The face sheets and core of the sandwich beams were manufactured from AISI type 304 stainless-steel sheet of thickness 0.3 mm and density $\rho_f = 7900\,\mathrm{kg\,m^{-3}}$. Both the Y-frame and corrugated cores were manufactured with an effective density $\rho_c \approx 200\,\mathrm{kg\,m^{-3}}$ and core depth $c = 22\,\mathrm{mm}$. Consequently, the effective relative density of the cores is $\bar{\rho} = 2.5\%$. All sandwich beams had an areal mass of magnitude $m = 2t\rho_f + c\rho_c \approx 10\,\mathrm{kg\,m^{-2}}$.

In order to define the core orientation, we introduce a local coordinate system $(x_1, x_2, x_3)$ for the core, and a

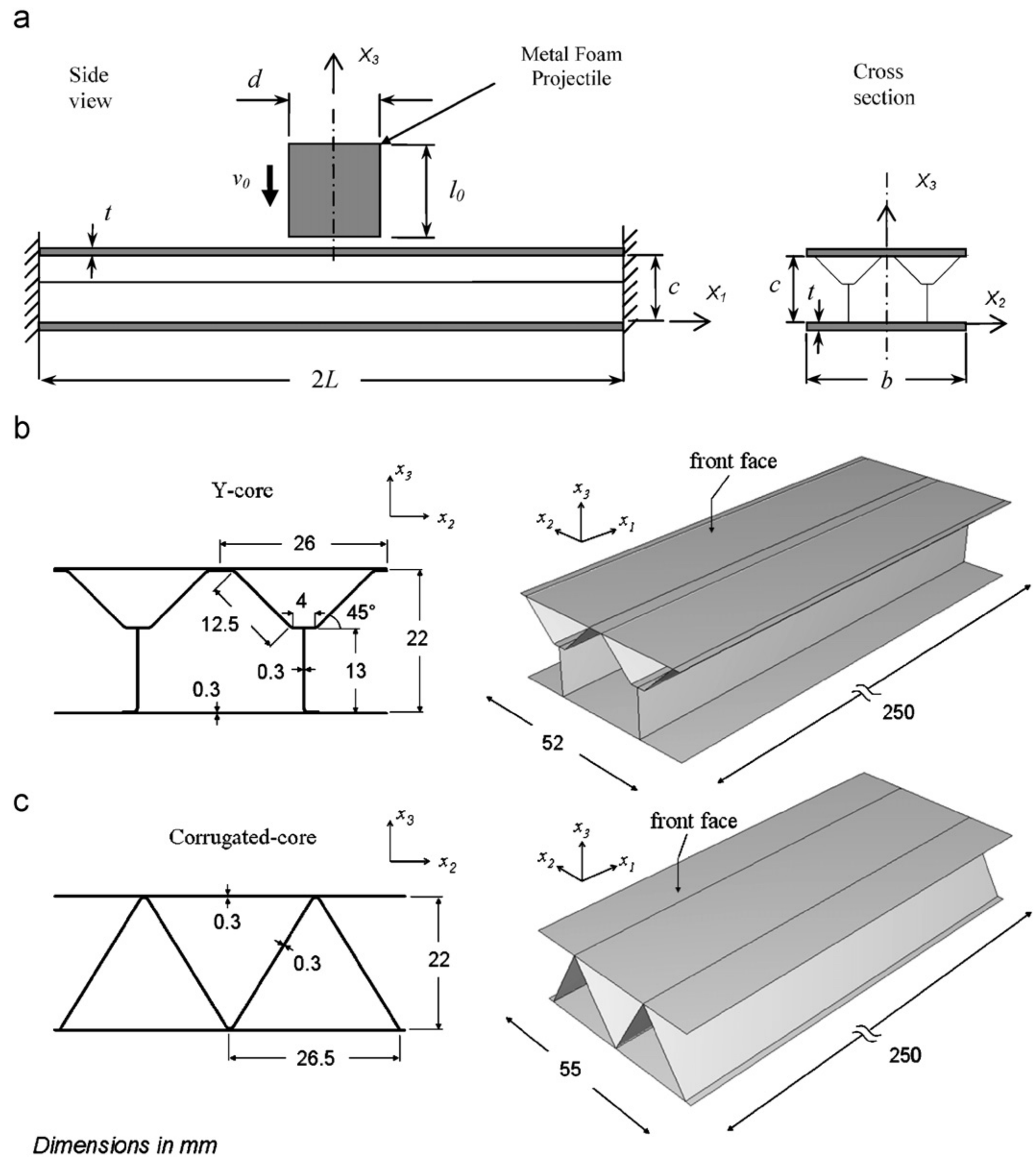


Fig. 2. (a) Sketch of the clamped Y-frame core sandwich beam geometry (longitudinal core orientation) and the loading arrangement. Geometries of the (b) Y-frame and (c) corrugated sandwich cores. All dimensions are in mm and both local and global co-ordinate systems employed are defined.

global co-ordinate system $(X_1, X_2, X_3)$ for the beam, see Fig. 2. $x_1$ is the prismatic direction for the core, $x_2$ is the transverse direction of the core, and $x_3 = X_3$ is the out-of-plane direction. Both the Y-frame and the corrugated cores were close-packed in the $x_2$ direction, such that adjacent frames touched. In the *longitudinal* configuration, the core comprised two Y-frame or corrugated core sections, with the longitudinal $x_1$-axis of the core parallel to the longitudinal $X_1$-axis of the beam. These beams had a span $2L = 250$ mm and width $b = 52$ and 55 mm (in the $X_2$-direction) for the Y-frame and corrugated core beams, respectively. In the *transverse* orientation, 10 corrugated or Y-frame sections were arranged with the transverse $x_2$-axis of the core along the longitudinal axis ($X_1$-axis) of the beam. The sandwich beams with a transverse core orientation had a span $2L = 260$ mm, giving an integer number of corrugations and Y-frame sections along the beam length. The width was $b = 52$ mm in the $X_2$-direction.

The longitudinal and transverse beams were end-clamped as shown in Fig. 3. To facilitate this, the beams were manufactured with an overall length of 375 mm. The longitudinal beams were produced individually. In contrast, the transverse beams were produced in batches, first by manufacturing rectangular sandwich plates of plan dimension $300\,\text{mm} \times 375\,\text{mm}$, and second by water-jet cutting these plates into beams of length 375 mm and width $b = 52$ mm.

### 2.1.1. Y-frame core

Stainless-steel sheets were computer-numerical-control (CNC) folded to form the upper part of the Y-frame and the Y-frame leg. Slots were CNC cut into the Y-frame web

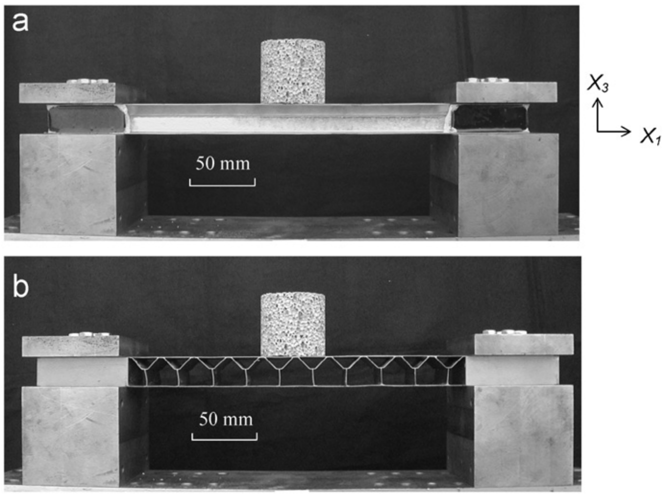


Fig. 3. Photographs of the clamped Y-frame sandwich beams. (a) Longitudinal and (b) transverse core arrangements in dynamic loading rig.

and the Y-frame leg was then fitted into the upper part of the Y-frame, as described in [12]. The core was spot welded to the face sheets and the braze alloy Ni–Cr 25-P10 (wt%) was applied in powder form over all sheets of the assembly. The assembly was then brazed together in a vacuum furnace at 1075 °C in a dry argon atmosphere at 0.03–0.1 mbar. A selected number of Y-frame sandwich beams were also manufactured by laser welding together the Y-frame components and then laser welding the core to the sandwich beam face sheets. These specimens were used to investigate the effect of manufacturing route upon the observed dynamic failure mode. Unless otherwise mentioned, all results are presented for the Y-frame sandwich beams as manufactured by the brazing route.

### *2.1.2. Corrugated core*

The corrugated core comprising struts inclined at $\pm 60^\circ$ (Fig. 2c) was manufactured by CNC folding 0.3 mm thick 304 stainless-steel sheets. This folded section was then brazed to 0.3 mm thick face sheets. Both transverse and longitudinal beams were manufactured following the same protocol as for the Y-frame.

### *2.1.3. Grippage of the specimens*

Photographs of the Y-frame sandwich beams in the *longitudinal* and *transverse* core arrangements, along with the metal foam projectiles used to load these beams, are shown in Fig. 3. In order to achieve a fully clamped boundary condition on the beam ends, the end portions of length 60 mm were bolted onto the test rig. Provision was made for grippage of the ends of the beam by making the sandwich core fully dense between the grips by the following technique. In the longitudinal arrangement, the sandwich core at the ends of the beams was filled with an epoxy resin. In the transverse arrangement, the core existed only within the span length of 260 mm of the beams, and metal inserts of depth $c = 22$ mm and length 60 mm were placed between the two face sheets at their ends. For both types of grippage, the end portions of the sandwich beams were bolted to the test-rig via steel clamping plates and M6 bolts, as shown in Fig. 3.

Dynamic tests were also performed on AISI 304 stainless-steel monolithic beams of areal mass $m \approx 10\,\mathrm{kg\,m^{-2}}$ (i.e. thickness $h = 1.2$ mm) equal to that of the sandwich specimens. These monolithic beams were coated with the same braze alloy as used in sandwich beam construction, and were subjected to the same thermal cycle: this ensures that the monolithic beams have the same composition and microstructure as that of the sandwich beams. The monolithic beams were gripped to the test-rig using the arrangement shown in Fig. 3.

## *2.2. Properties of the constituent materials*

The out-of-plane compressive responses of the Y-frame and corrugated core sandwich specimens were measured at a nominal strain rate of $10^{-3}\,\mathrm{s}^{-1}$. The loading direction was normal to the plane of the face sheet, and no relative sliding of the face sheets was permitted, see Rubino et al. [14] for details of the experimental procedure. The measured compressive nominal stress $\sigma_n$ versus nominal strain $\varepsilon_n$ responses are plotted in Fig. 4a, and show that the Y-frame and corrugated cores (of 2.5% relative density) exhibit a peak compressive strength of approximately 0.9 MPa followed by a softening response. Both cores show a second sharp increase in strength at a nominal strain of approximately 0.8. We shall refer to the strain level at which 'lock-up' occurs as the densification strain $\varepsilon_D$. Readers are referred to Rubino et al. [12] and Côté et al. [14] for further information on the quasi-static response of the Y-frame core and corrugated cores, respectively.

The typical uniaxial compressive response of Alporas metal foam of relative density $\bar{\rho} \approx 0.11$ is included in Fig. 4b; this foam was used for manufacture of the foam projectiles in the dynamic experiments. The quasi-static compressive response of the foam at a strain rate of $10^{-3}\,\mathrm{s}^{-1}$ was measured on a cylindrical specimen of diameter 50.8 mm and length 50 mm. The foam has a plateau strength of approximately 2.5 MPa and a nominal densification strain of $\varepsilon_D \approx 0.8$. The measured compressive response of the foam is used as an input to the FE simulations of sandwich beam impact. In brief, a rate-dependent elastic–plastic response was assumed with yield surface dependant upon mean stress and von Mises effective stress. See Deshpande and Fleck [21] for full details of the constitutive description for the metallic foam.

Tensile specimens of standard dog-bone geometry were cut from the as-received 304 stainless-steel material and were subjected to the same brazing cycle as that used to manufacture the sandwich and monolithic beams. The measured true stress versus logarithmic plastic strain curve $\sigma_0(\varepsilon^p)$ for the AISI 304 stainless steel at an applied strain rate $10^{-3}\,\mathrm{s}^{-1}$ is shown in Fig. 5a. The material can be regarded as elastic, linearly hardening with Young's

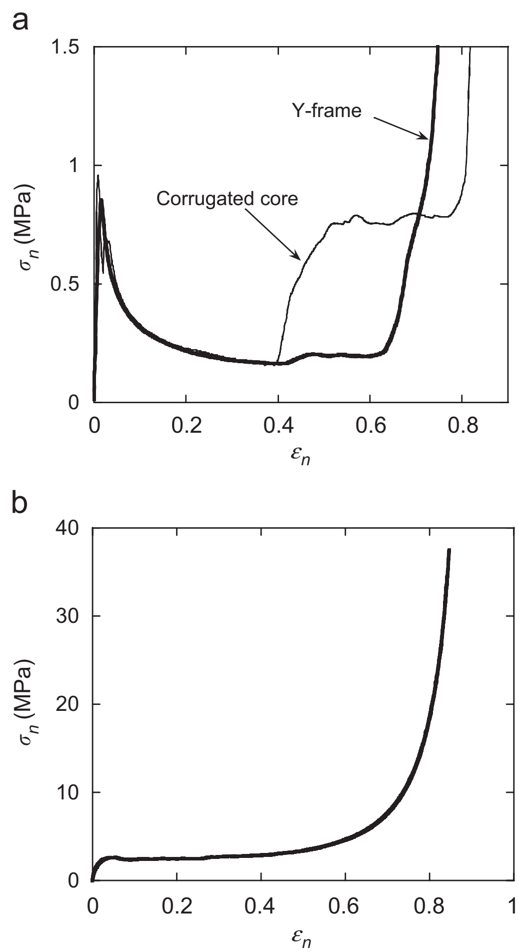


Fig. 4. (a) Measured quasi-static compressive stress versus strain responses of Y-frame and corrugated sandwich cores. (b) The quasi-static nominal compressive stress versus nominal strain response of the Alporas metal foam.

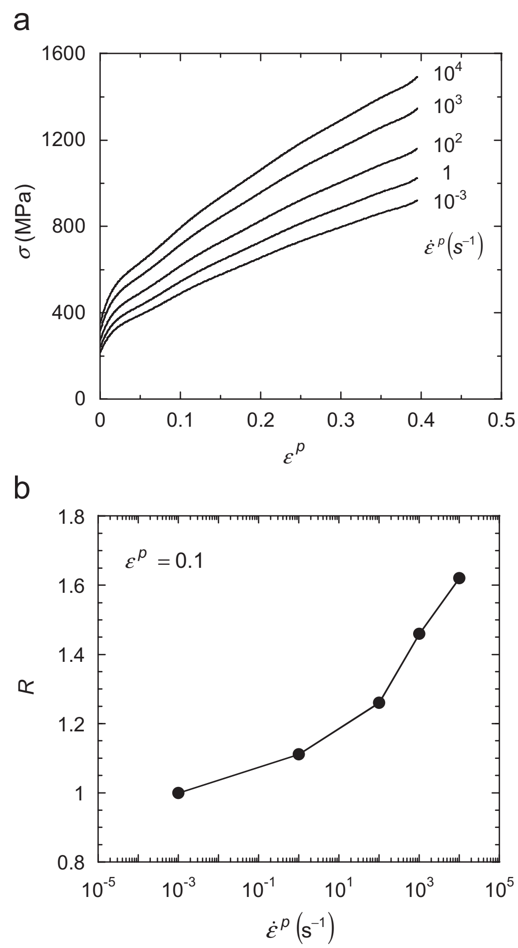


Fig. 5. (a) The measured quasi-static ($\dot{\varepsilon}^p = 10^{-3}\,s^{-1}$) tensile stress versus strain response of the AISI 304 stainless steel and the estimated high strain rate response at four additional values of strain rate, using the data of Stout and Follansbee (1986). (b) The dynamic strength enhancement ratio $R$ as a function of plastic strain rate $\dot{\varepsilon}^p$ for the AISI 304 stainless steel at a plastic strain $\varepsilon^p = 0.1$.

modulus $E = 210\,\text{GPa}$ and yield strength $\sigma_Y = 210\,\text{MPa}$. Knowledge of the high strain rate response of the 304 stainless-steel sheets is needed for the FE simulations. Stout and Follansbee [22] have investigated the strain-rate sensitivity of the AISI 304 stainless steel for strain rates in the range $10^{-4}\,s^{-1} < \dot{\varepsilon} < 10^4\,s^{-1}$. Their data are re-plotted in Fig. 5b, where the dynamic strength enhancement ratio $R$ is plotted against the plastic strain rate $\dot{\varepsilon}^p$ for $10^{-3}\,s^{-1} < \dot{\varepsilon}^p < 10^4\,s^{-1}$. Here, $R$ is defined as the ratio of the stress $\sigma_d(\varepsilon^p = 0.1)$ at an applied strain rate $\dot{\varepsilon}^p$ to the stress $\sigma_0(\varepsilon^p = 0.1)$ at an applied $\dot{\varepsilon}^p = 10^{-3}\,s^{-1}$. The measured stress versus strain histories presented in [22] indicate that $R$ is reasonably independent of the choice of plastic strain $\varepsilon^p$ at which $R$ is calculated. Thus, the dynamic strength $\sigma_d$ versus plastic strain $\varepsilon^p$ history can be estimated as

$$\sigma_d = R(\dot{\varepsilon}^p)\sigma_0(\varepsilon^p, ) \tag{1}$$

where $R(\dot{\varepsilon}^p)$ is given in Fig. 5b. In the dynamic FE simulations of the experiments presented in Section 4, we employ this prescription for the strain-rate sensitivity of the stainless steels, with $\sigma_0(\varepsilon^p)$ given by the measured quasi-static stress versus strain history (Fig. 5a). For illustration, the estimated true tensile stress versus logarithmic plastic strain histories of the AISI 304 stainless steel are sketched in Fig. 5a for four values of applied strain rate in addition to the measured response at $\dot{\varepsilon}^p = 10^{-3}\,s^{-1}$.

### 2.3. Protocol for the dynamic tests

Alporas aluminium foam projectiles of length $l_0 \approx 50\,\text{mm}$ were used to impact the clamped monolithic and sandwich beams over a central circular patch of diameter $d = 50.8\,\text{mm}$, as shown in Fig. 2a. The use of foam projectiles as a means of providing a well-characterised pressure versus time loading pulse has been developed by Radford et al. [18] and subsequently employed to investigate the dynamic response of sandwich beams with lattice cores [19] and circular sandwich plates with metal foam cores [23] and lattice cores [24].

The circular cylindrical projectiles were electro-discharge machined from Alporas foam blocks of density

$\rho_p = 300\,\mathrm{kg\,m^{-3}}$. The projectiles were fired at a velocity $v_0$ in the range 30–426 m s$^{-1}$ from a gas gun of bore 50.8 mm and barrel length 4.5 m, providing a projectile momentum per unit area $I_0 = \rho_p l_0 v_0$ of up to 6.4 kN s m$^{-2}$. The velocity of the projectile was measured at the exit of the barrel using laser-velocity gates. The impacted faces of the Y-frame and corrugated core sandwich beams are displayed in Fig. 2: in keeping with the Y-frame structures used in ships constructed by Schelde Shipbuilding, the web of the Y-frame was adjacent to the impacted face of the beam, while the Y-frame leg was attached to the non-impacted face of the sandwich beam. Tables 1 and 2 summarise the tests performed on the sandwich beams in the longitudinal and transverse core arrangements, respectively, with details given on the projectile impact velocity and initial projectile momentum. High-speed photography was used to observe the dynamic transverse deformation of the beams. A Hadland Imacon-790 image-converter camera was used with inter-frame times and exposure times of 100 and 20 μs, respectively. Post-test, the beams were examined to measure the permanent mid-span deflection and to determine the level of projectile momentum, which led to the initiation of failure.

The key metrics used to characterise the performance of the beams are (i) the maximum/permanent deflection of the dry face: in marine construction; (ii) core compression and (iii) the maximum plastic strains in the beams as inferred from the FE calculations. These three metrics combined give some indication of the relative performances of the sandwich and monolithic beams. In these experiments,

Table 1
The measured dynamic response of monolithic and sandwich beams (longitudinal core orientation)

| Specimen | Projectile | | Response | | |
|---|---|---|---|---|---|
| | $I_0=\rho_p l_0 v_0$ (kN s m$^{-2}$) | $v_0$ (ms$^{-1}$) | $w_b$ (mm) | $\varepsilon_c$ | Failed |
| Monolithic | 1.6 | 110 | 25 | – | - |
| | 3.0 | 200 | 37 | – | – |
| | 4.6 | 305 | 50.5 | – | – |
| | 5.4 | 360 | 59 | – | – |
| | 6.3 | 420 | X | – | Yes |
| As-brazed Y-core | 1.6 | 109 | 9 | 0.52 | – |
| | 3.0 | 199 | 21 | 0.77 | – |
| | 4.5 | 301 | 45 | 0.75 | Yes |
| | 4.9 | 327 | X | X | Yes |
| | 5.4 | 360 | X | X | Yes |
| Corrugated | 1.6 | 110 | 9 | 0.49 | – |
| | 2.9 | 193 | 18 | 0.68 | – |
| | 4.5 | 303 | 39 | 0.84 | – |
| | 5.4 | 360 | 47 | 0.86 | – |
| | 6.4 | 426 | X | X | Yes |

The symbol X denotes separation of the beam into two or more pieces.

Table 2
The measured dynamic response of monolithic and sandwich beams (transverse core orientation)

| Specimen | Projectile | | Response | | |
|---|---|---|---|---|---|
| | $I_0=\rho_p l_0 v_0$ (kN s m$^{-2}$) | $v_0$ (ms$^{-1}$) | $w_b$ (mm) | $\varepsilon_c$ | Failed |
| Monolithic | 0.5 | 31 | 22 | – | – |
| | 1.5 | 98 | 26 | – | – |
| | 2.3 | 154 | 36 | – | – |
| | 3.0 | 198 | 40 | – | – |
| As-brazed Y-core | 0.7 | 49 | 20 | 0.16 | – |
| | 1.5 | 99 | 23 | 0.31 | Yes |
| | 2.3 | 154 | 29 | 0.67 | Yes |
| | 3.1 | 204 | X | X | Yes |
| Corrugated | 0.9 | 63 | 18 | 0.3 | – |
| | 1.5 | 99 | 21 | 0.4 | – |
| | 2.3 | 154 | 29 | 0.6 | Yes |
| | 2.9 | 194 | 59 | 0.7 | Yes |

The symbol X denotes separation of the beam into two or more pieces.

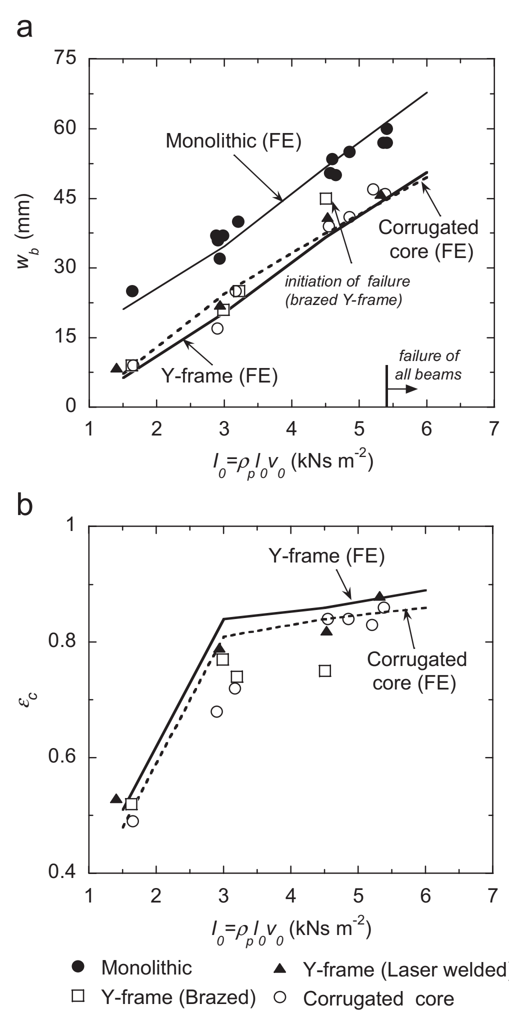


Fig. 6. Comparison of the measured and predicted permanent (a) rear-face deflections and (b) core compression at mid-span of the dynamically loaded monolithic and sandwich beams (longitudinal core orientation), as a function of the foam projectile momentum $I_0$. The symbols denote measurements and the continuous lines denote FE predictions.

energy absorption capacity of the beams is not an appropriate performance metric, a significant fraction of the initial kinetic energy of the metal foam projectile is dissipated in the deformation of the projectile itself. Moreover, the deformation of the projectile is dependent on the structural rigidity of the target beam (i.e. the deformation of the projectile increases with increasing rigidity of the target) and thus energy absorption by the beam is not a suitable measure to compare performances.

## 3. Experimental results

The sensitivity of beam deflection to the initial momentum $I_0$, manufacturing route of the Y-frame core and the orientation of the sandwich cores (longitudinal versus transverse) was investigated. At least four levels of initial momentum were applied to each specimen configuration by varying the impact velocity of the foam projectiles (Tables 1 and 2). Spot repeat tests were conducted to confirm the reproducibility of the measurements reported here. We also note that in nearly all the tests the foam projectiles underwent complete densification during the impact event.

### *3.1. Effect of projectile momentum upon the deformation of monolithic beams and sandwich beams with a longitudinal core*

The shock responses of the monolithic beams and of the sandwich beams with a longitudinal core are compared in Fig. 6a; the figure contains a plot of the permanent rear-face deflections at mid-span $w_b$ versus the initial momentum of the foam projectile $I_0$ for beams of span $2L = 250\,\text{mm}$.

The time evolution of the deformation and failure of the brazed Y-frame and corrugated core sandwich beams is shown in Figs. 7 and 8, respectively, via high-speed photographs. For each topology, results are presented for $I_0 \approx 3$ and $5.4\,\text{kN}\,\text{s}\,\text{m}^{-2}$. Time is measured from the instant of foam impact. Travelling plastic hinges initiate at the impact location and travel towards the beam supports; these are clearly visible for the $I_0 \approx 3\,\text{kN}\,\text{s}\,\text{m}^{-2}$ tests (Figs. 7a and 8a). When these hinges reach the beam

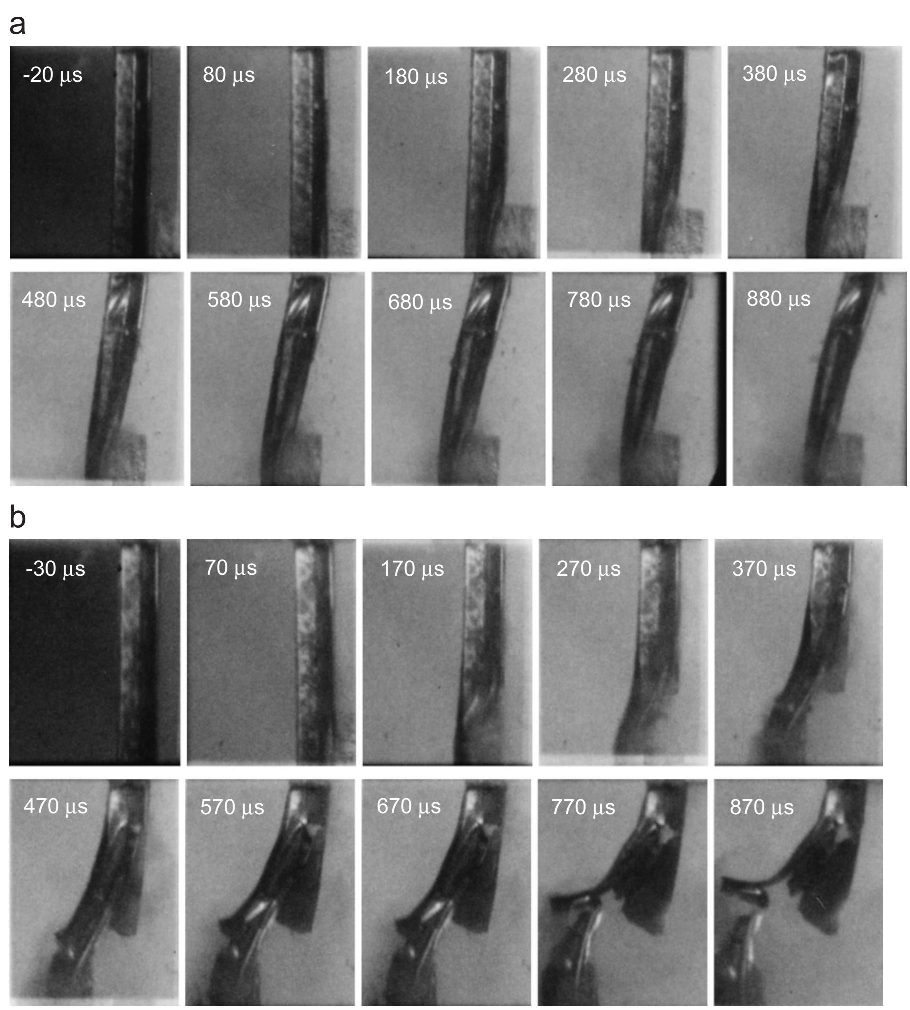


Fig. 7. High-speed photographic sequence of the deformation of the Y-frame sandwich beams (longitudinal core orientation) for (a) $I_0 = 3\,\text{kN}\,\text{s}\,\text{m}^{-2}$ and (b) $I_0 = 5.4\,\text{kN}\,\text{s}\,\text{m}^{-2}$. The inter-frame time is 100 μs and time $t$ is measured from the instant of the impact.

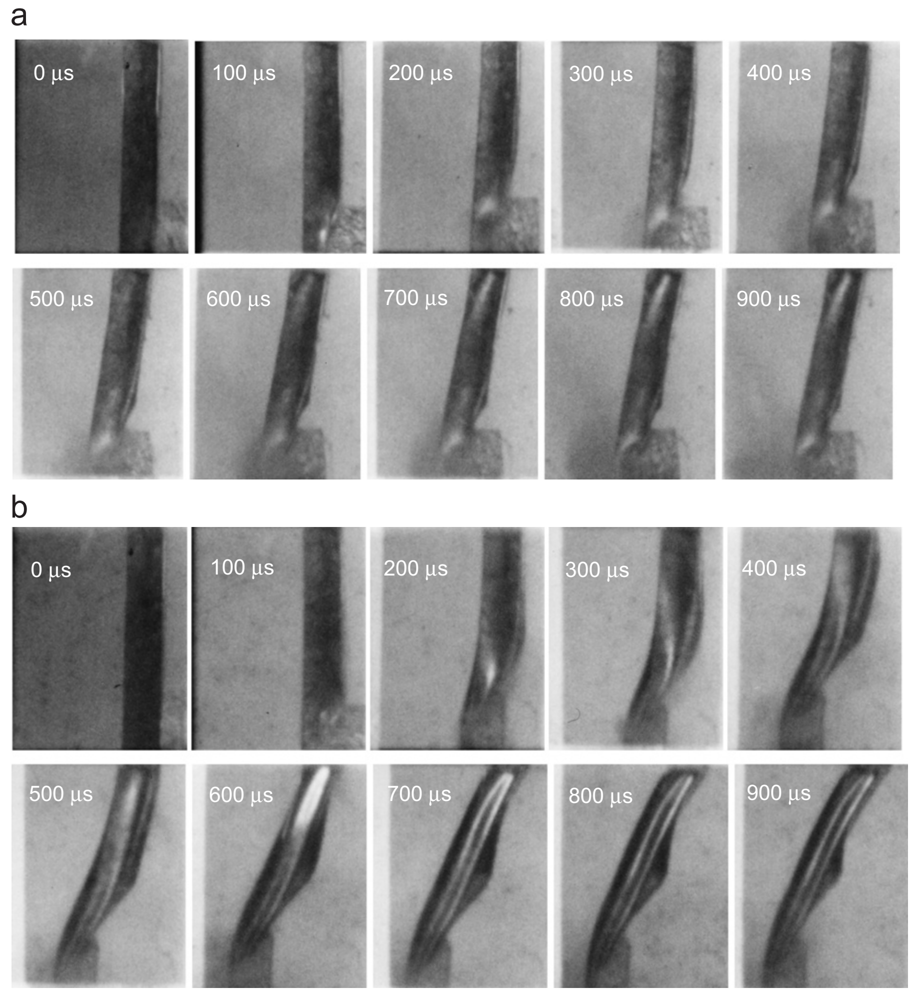


Fig. 8. High-speed photographic sequence of the deformation of the corrugated core sandwich beams (longitudinal core orientation) for (a) $I_0 = 2.9\,\mathrm{kN\,s\,m^{-2}}$ and (b) $I_0 = 5.4\,\mathrm{kN\,s\,m^{-2}}$. The inter-frame time is 100 μs and time $t$ is measured from the instant of the impact.

supports, large shear deformations ensue in the core and result in wrinkling of the cores. However, these deformations do not result in beam failure. For the choice $I_0 = 5.4\,\mathrm{kN\,s\,m^{-2}}$, the front face of the Y-frame sandwich beam begins to tear near the edge of the foam impact site before the travelling plastic hinges have reached the beam supports (Fig. 7b). Complete failure of the Y-frame sandwich beam follows. In contrast, the corrugated core sandwich beam remains intact (Fig. 8b).

Photographs of the final deformed profiles of the monolithic and sandwich beams are summarised as a montage in Fig. 9. The travelling plastic hinges result in continuously curved profiles of the dynamically tested beams, as clearly evidenced from the photographs of the monolithic beams in Fig. 9a. In contrast, the sandwich beams deform by a combination of beam bending and core compression, see Figs. 9b and 9c.

The various types of beam failed at sufficiently high impulses, as follows:

(i) The as-brazed Y-frame tore at $I_0 \geqslant 4.5\,\mathrm{kN\,s\,m^{-2}}$. The front face and core tore near the supports, while the back face and core tore near mid-span.

(ii) The laser-welded Y-frame, corrugated core and monolithic beams failed at $I_0 \geqslant 6.4\,\mathrm{kN\,s\,m^{-2}}$. In all cases, failure involved tensile tearing across the section of the beam.

It is instructive to compare the impact responses of the monolithic and sandwich beams in the regime of no failure, $I_0 < 4.5\,\mathrm{kN\,s\,m^{-2}}$. It is clear from Fig. 6a that the sandwich beams with a corrugated core and a Y-core outperform the monolithic beams of equal areal mass. Define the core compressive strain as $\varepsilon_c \equiv \Delta c/c$, where $\Delta c$ is the reduction in core thickness averaged over the beam width $b$, at mid-span; the dependence of $\varepsilon_c$ upon $I_0$ is plotted in Fig. 6b for the two sandwich beam configurations. The strain $\varepsilon_c$ increases with increasing $I_0$ up to $I_0 \approx 3\,\mathrm{kN\,s\,m^{-2}}$; at higher imposed impulses the core compression is approximately constant at its densification value of 0.8 for both the Y-frame and corrugated cores. The responses of the brazed and laser-welded Y-frame sandwich beams are nearly identical for $I_0 < 4.5\,\mathrm{kN\,s\,m^{-2}}$.

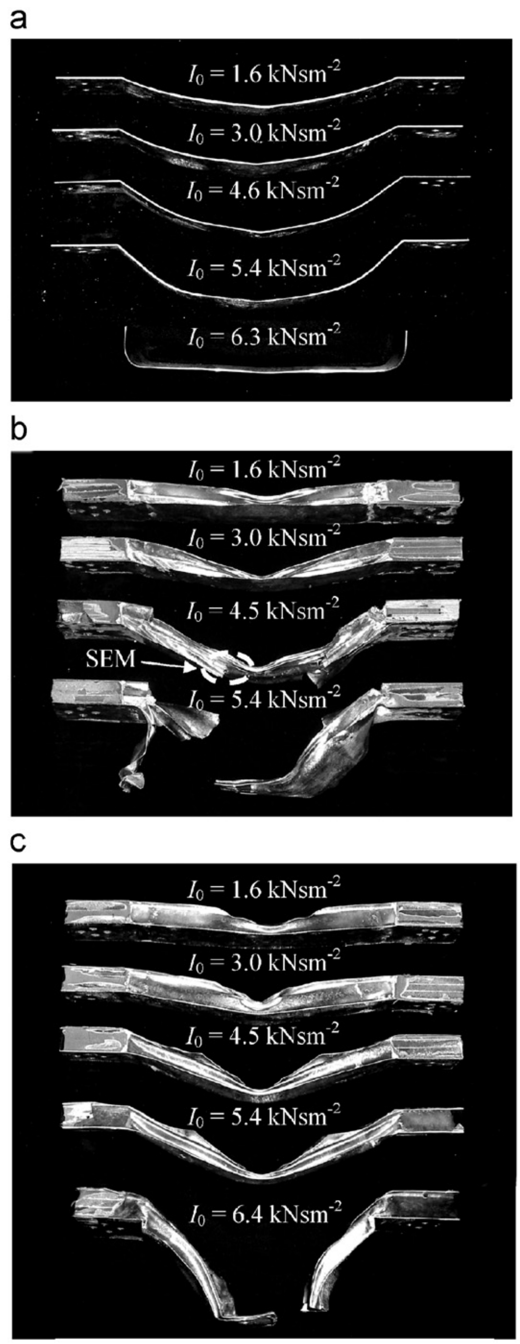


Fig. 9. Photographs showing the deflected profiles of the dynamically loaded (a) monolithic (b) Y-frame and (c) corrugated core sandwich beams (longitudinal core orientation) at selected values of foam projectile momentum $I_0$.

## 3.2. *Effect of brazing on failure of the Y-frame sandwich beams*

Uniformly distributed phosphides are present in the brazed joints as discussed by Côté et al. [25] in the context of the brazed diamond core lattice. These phosphides decrease the ductility of the joints. Typically, cracks initiate at the interface between core struts and the face sheet of the dynamically tested Y-frame sandwich beams and propagate across the section of the face sheet. A representative scanning electron microscope image of the joint detail is given in Fig. 10a with a magnified view of the joint between the Y-frame leg and the rear face sheet shown in Fig. 10b. A crack initiates in the joint and then propagates by micro-void coalescence through the thickness of the face sheet. The V-shaped geometry of the joint between the corrugated core and the face sheet draws braze alloy into the joints of the corrugated core beam, making them stronger than the joint between the Y-frame leg and the rear face sheet. Consequently, the brazed Y-frame sandwich beam fails at a lower impact velocity than the corrugated beam.

Photographs of the deformed profiles of the brazed and laser-welded Y-frame sandwich beams impacted at $I_0 \approx 5.4\,\mathrm{kN\,s\,m^{-2}}$ are included in Figs. 11a and b, respectively. Intense shear deformation of the Y-frame core occurs in the laser-welded Y-frame sandwich beams and results in wrinkling but in no visible tearing. The brazed Y-frame sandwich beam tears at $I_0 \geqslant 4.5\,\mathrm{kN\,s\,m^{-2}}$, while the laser-welded Y-frame and brazed corrugated beams tear at $I_0 \geqslant 6.4\,\mathrm{kN\,s\,m^{-2}}$ (Fig. 11b). The front face detaches from the core at the laser weld near the supports of the Y-frame specimen at $I_0 = 6.4\,\mathrm{kN\,s\,m^{-2}}$. This comparison reveals that brazing of the Y-core leads to a reduction in its dynamic strength due to premature failure at the joints.

## 3.3. *Effect of prismatic core orientation upon dynamic strength*

The corrugated and Y-frame sandwich cores are highly anisotropic: the longitudinal stretching strength $\sigma_{11}^{Y}$ much exceeds the transverse strength $\sigma_{22}^{Y}$, and similarly the longitudinal shear strength $\sigma_{13}^{Y}$ is much greater than the transverse shear strength $\sigma_{23}^{Y}$. Thus, we expect the response of the sandwich beam to be sensitive to the orientation of the $x_1$-axis of the cores relative to the longitudinal axis ($X_1$-axis) of the sandwich beam. Results have already been given above for tests with cores in the longitudinal direction. Corrugated core and Y-frame core sandwich beams with the transverse core orientation were tested dynamically over a foam projectile momentum range $0.5\,\mathrm{kN\,s\,m^{-2}} \leqslant I_0 \leqslant 3\,\mathrm{kN\,s\,m^{-2}}$.

The measured permanent mid-span rear-face deflections $w_b$ are plotted in Figs. 12a and b for the Y-frame and corrugated core sandwich beams (transverse core orientation), respectively. Numerical fits through the data for the rear-face deflection of the sandwich beams in the longitudinal core orientation (Fig. 6a) are included in Figs. 12a and 12b for comparison purposes. Also shown are the permanent mid-span deflections of the monolithic beams (span $2L = 260\,\mathrm{mm}$) for the same areal mass as that of the sandwich beams. We note that the sandwich beams with transversely orientated corrugated and Y-frame cores have rear-face deflections that are only slightly less than their

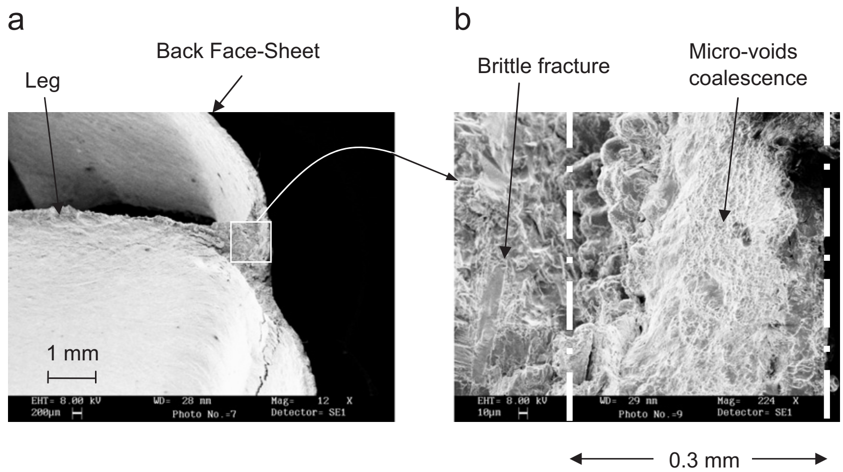


Fig. 10. (a) A representative scanning electron microscope (SEM) image of the failed joint between the Y-frame leg and the rear face sheet of the brazed Y-frame sandwich beam tested at $I_0 = 4.5\,\mathrm{kNsm}^{-2}$ (see Fig. 9b). (b) A magnified view of the joint.

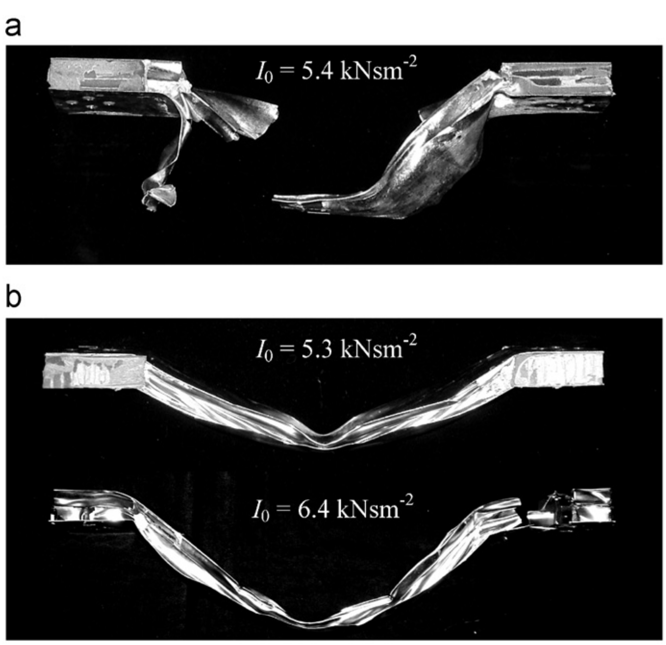


Fig. 11. Photographs showing a comparison of the final deformed profiles of the (a) brazed and (b) laser-welded Y-frame sandwich beams (longitudinal core orientation) at high foam projectile impact momentums $I_0$. The brazed beam fails at $I_0 = 5.4\,\mathrm{kN\,s\,m}^{-2}$, while failure initiates in the laser-welded beams at $I_0 = 6.4\,\mathrm{kN\,s\,m}^{-2}$.

monolithic counterparts.[2] We attribute the relatively poor performance of the sandwich beams with the transversely oriented cores to the low shear and stretch strengths of the cores along the longitudinal axis of the beam, see Fleck and Deshpande [6] for a discussion on the effect of core strength on the dynamic performance of clamped beams. In contrast, the sandwich beams of longitudinal core orientation consistently outperform monolithic beams of equal mass. Both types of sandwich beams with transverse core orientation fail at $I_0 \approx 3\,\mathrm{kN\,s\,m}^{-2}$, which is less than the impulsive strength of the monolithic beams of equal mass.

The ratio of measured back face deflection of the sandwich beam to that of monolithic beam (of same mass) $w_{\mathrm{sandwich}}/w_{\mathrm{monolithic}}$ is plotted as a function of projectile momentum $I_0$ in Fig. 12c. It is concluded that the deflections of the Y-frame and corrugated core sandwich beams are broadly similar. Sandwich beams of longitudinal orientation outperform monolithic beams particularly at low impulse levels.

High-speed photographic sequences of the deformed sandwich beams with transverse orientations of Y-frame and corrugated core are shown in Figs. 13 and 14, respectively. In part (a) of each figure, photographs are shown for $I_0 = 1.5\,\mathrm{kN\,s\,m}^{-2}$, while in part (b), photographs are given for $I_0 \approx 3\,\mathrm{kN\,s\,m}^{-2}$. The high-speed photographs reveal (i) travelling plastic hinges, (ii) high levels of core compression beneath the foam projectile and (iii) intense shear deformations in the core for both sandwich beams. At $I_0 \approx 3\,\mathrm{kNsm}^{-2}$, the Y-frame sandwich beam undergoes significantly larger deformation than the corrugated core beam. In fact, the Y-frame beam fails approximately 1 ms after impact (not shown), while only the initiation of failure is observed in the corrugated core beam.

Photographs of the final deformed profiles of the sandwich beams at selected impact momentums are given in Fig. 15. For both types of sandwich core, shear deformation of the core is evident over the beam length along with compression of the core near mid-span. Moreover, the beams that do not fail display a

[2]Recall that the sandwich beams with the transverse core orientation have a span $2L = 260\,\mathrm{mm}$, while the sandwich beams with the longitudinal core orientation have a span of 250 mm. The slightly longer span of sandwich beams with the transverse core orientation however cannot account for the significantly higher deflections of these beams; for example the deflections of the monolithic beams with spans of 250 and 260 mm in Figs. 6a and 12a are comparable.

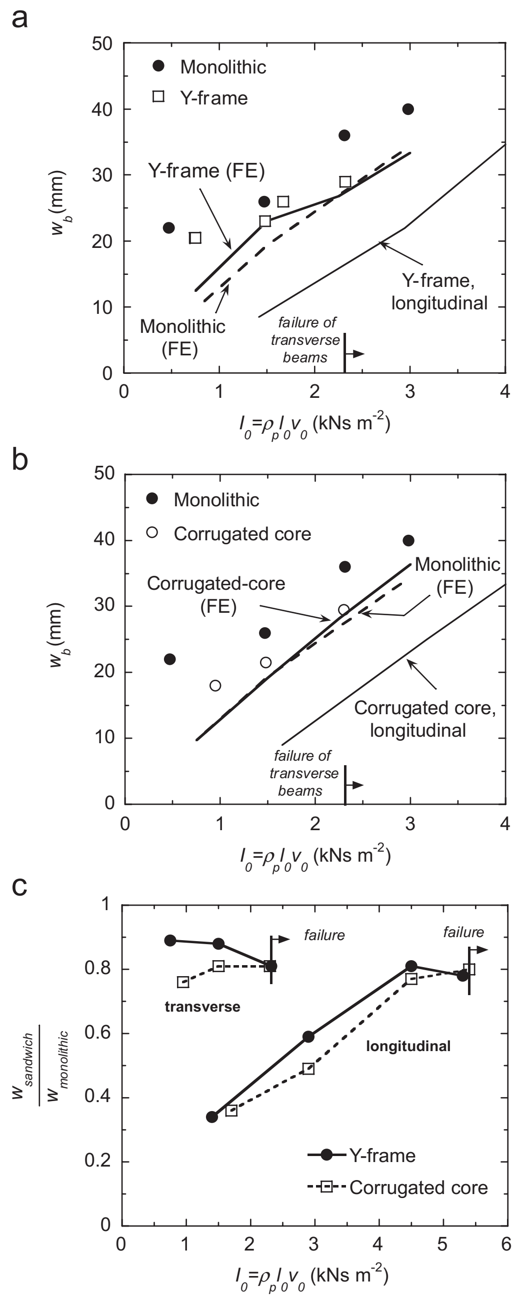


Fig. 12. Effect of projectile momentum upon the measured and predicted mid-span, rear-face deflection of the dynamically loaded monolithic and sandwich beams. (a) Y-frame and (b) corrugated core beams with transverse core orientation. The symbols are measurements and the continuous lines are FE predictions. The measurements for the sandwich beams with the longitudinal core orientation are taken from Fig. 6a. (c) The ratio of measured rear-face deflection of sandwich beam to monolithic beam is plotted versus $I_0$.

continuously curved profile resulting from deformation by the travelling hinge deformation mode. We note that failure initiates in the Y-frame and corrugated core beams at $I_0 \approx 1.5$ and $I_0 \approx 2.3\,\mathrm{kN\,s\,m^{-2}}$, respectively. As discussed in Section 3.2, we attribute this difference to the fact that the brazed joints of the Y-frame beams are relatively weak compared with the V-shaped joints of the corrugated core beams.

## 4. Finite element simulations

Comparisons of the FE predictions and the measured responses of the monolithic and sandwich beams are presented in this section. All computations were performed using the explicit time integration version of the commercially available FE code ABAQUS[3] (version 6.4). Here we briefly describe the details of these FE calculations.

Three-dimensional simulations of the sandwich and monolithic beams were performed. Symmetry boundary conditions were prescribed at mid-span ($X_1 = 0$) and on the mid-plane $X_2 = 0$, see Fig. 2a. Clamped boundary conditions were imposed on the beams at $X_1 = L$ by constraining to zero all nodal rotations and displacements. The validity of clamped boundary conditions to model the experimental situation is discussed subsequently in terms of the fidelity with which the simulations predict the observations. Dynamic loading was simulated by impact of a foam projectile: at the start of the simulation, the projectile was imparted an uniform velocity $v_o$ and was brought into contact with the beam at its mid-span. The "general contact" option in ABAQUS was employed to simulate contact between all adjacent surfaces. The general contact algorithm in ABAQUS enforced hard, no-friction contact interaction using a penalty algorithm.

The sandwich and monolithic beams were modelled using four-noded shell elements (S4R in ABAQUS notation) with reduced integration, hourglass control and five integration points through the thickness of the elements, for both the face sheets and the core. Perfect bonding between the core and face sheets was assumed. All dimensions (face sheet thickness and core dimensions) were chosen to match the experimental values, and an element size of 0.5 mm was employed for all calculations reported subsequently. The FE model comprised about 50,000 elements for the sandwich beams and 13,000 for the monolithic beams. The cylindrical foam projectiles of diameter 50.8 mm and length $l_0 = 50\,\mathrm{mm}$ were modelled using 30,000 linear hexahedral (C3D8R in ABAQUS notation) with the elements generated by sweeping about the cylindrical axis of the foam projectile. The projectiles had 50 elements in the axial direction and 25 elements along the radius.

### 4.1. Material properties

The AISI 304 stainless steel, as used for manufacture of the sandwich and monolithic beams, was treated as a J2-flow theory rate-dependent solid, of density $\rho_f = 7900\,\mathrm{kg\,m^{-3}}$, Young's modulus $E = 210\,\mathrm{GPa}$ and Poisson ratio $v = 0.3$. The uniaxial tensile true stress versus equivalent plastic strain curves at plastic strain rates $10^{-3}\,\mathrm{s^{-1}} \leqslant \dot{\varepsilon}^{p} \leqslant 10^{4}\,\mathrm{s^{-1}}$ were tabulated in ABAQUS using the prescription described in Section 2.2 and employing the data of Fig. 5. The strong strain hardening and high strain

[3]Hibbit, Karlsson and Sorensen Inc.

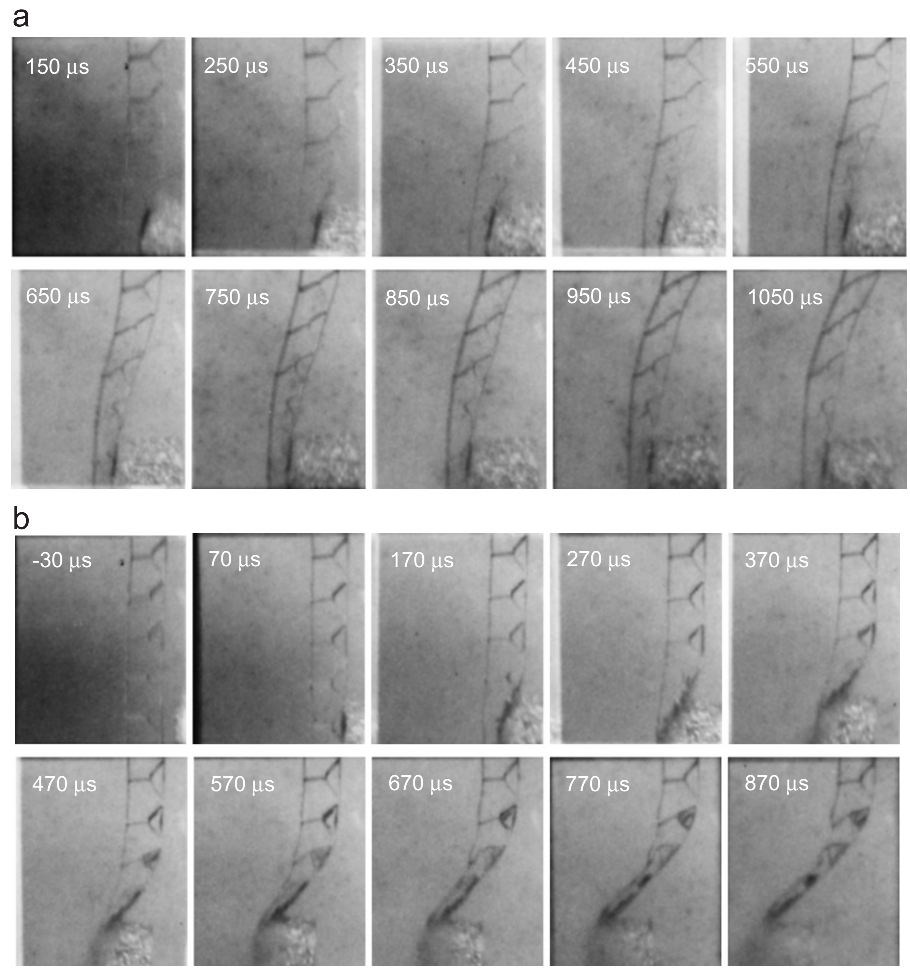


Fig. 13. High-speed photographic sequence of the deformation of the Y-frame sandwich beams (transverse core orientation). (a) $I_0 = 1.5\,\mathrm{kN\,s\,m^{-2}}$ and (b) $I_0 = 3.1\,\mathrm{kN\,s\,m^{-2}}$. The inter-frame time is 100 μs and time $t$ is measured from the instant of the impact.

rate sensitivity of the stainless steel prevents strong strain localisation in the FE calculations and reduces mesh sensitivity of the computations.

The metal foam projectile was modelled as a compressible continuum using a rate-dependent version of the constitutive model of Deshpande and Fleck [21]. An isotropic yield surface is specified by

$$\hat{\sigma} - Y = 0, \tag{2}$$

where the equivalent stress $\hat{\sigma}$ is a homogeneous function of the von Mises stress $\sigma_e$ and of the mean stress $\sigma_m \equiv \sigma_{kk}/3$ according to

$$\hat{\sigma}^2 \equiv \frac{1}{1+(\alpha/3)^2}[\sigma_e^2 + \alpha^2\sigma_m^2]. \tag{3}$$

As usual, the von Mises effective stress, $\sigma_e \equiv \sqrt{3s_{ij}s_{ij}/2}$, is a function of the deviatoric stress tensor $s_{ij}$. The yield stress $Y$ is specified by an over-stress model of the form

$$Y = \eta\dot{\hat{\varepsilon}}^p + \sigma_c, \tag{4}$$

in terms of the viscosity $\eta$. The plastic strain rate $\dot{\hat{\varepsilon}}^p$ is work conjugate to $\hat{\sigma}$. $\sigma_c(\hat{\varepsilon}^p)$ is the static uniaxial stress versus plastic strain relation. Normality of plastic flow is assumed, and this implies that the "plastic Poisson's ratio" $\nu_p = -\dot{\varepsilon}_{22}^p/\dot{\varepsilon}_{11}^p$ for uniaxial compression in the 1-direction is given by

$$\nu_p = \frac{1/2-(\alpha/3)^2}{1+(\alpha/3)^2}. \tag{5}$$

In the simulations, the Alporas foam is assumed to have a Young's modulus $E_c = 1.0\,\mathrm{GPa}$, an elastic Poisson's ratio $\nu = 0.3$ and a plastic Poisson ratio $\nu_p = 0$ [26]. The static yield strength $\sigma_c$ versus equivalent plastic strain $\hat{\varepsilon}^p$ history is calibrated using the compressive stress versus strain response presented in Fig. 4b. An over-stress model has the virtue of producing a plastic shock wave within the foam of finite width, as observed experimentally. The value of the viscosity $\eta$ was selected so that the shock width [18]

$$w = \frac{\eta\varepsilon_D}{\rho_p \Delta v}, \tag{6}$$

has the value of $l_0/10$. Recall that $l_0$ is the projectile length, and note that $\rho_p = 300\,\mathrm{kg\,m^{-3}}$ is the initial foam density, $\varepsilon_D$ is the nominal densification strain of the foam and $\Delta v$ is the velocity jump across the shock. For the purposes of this discussion, $\Delta v$ is approximately equal to the projectile

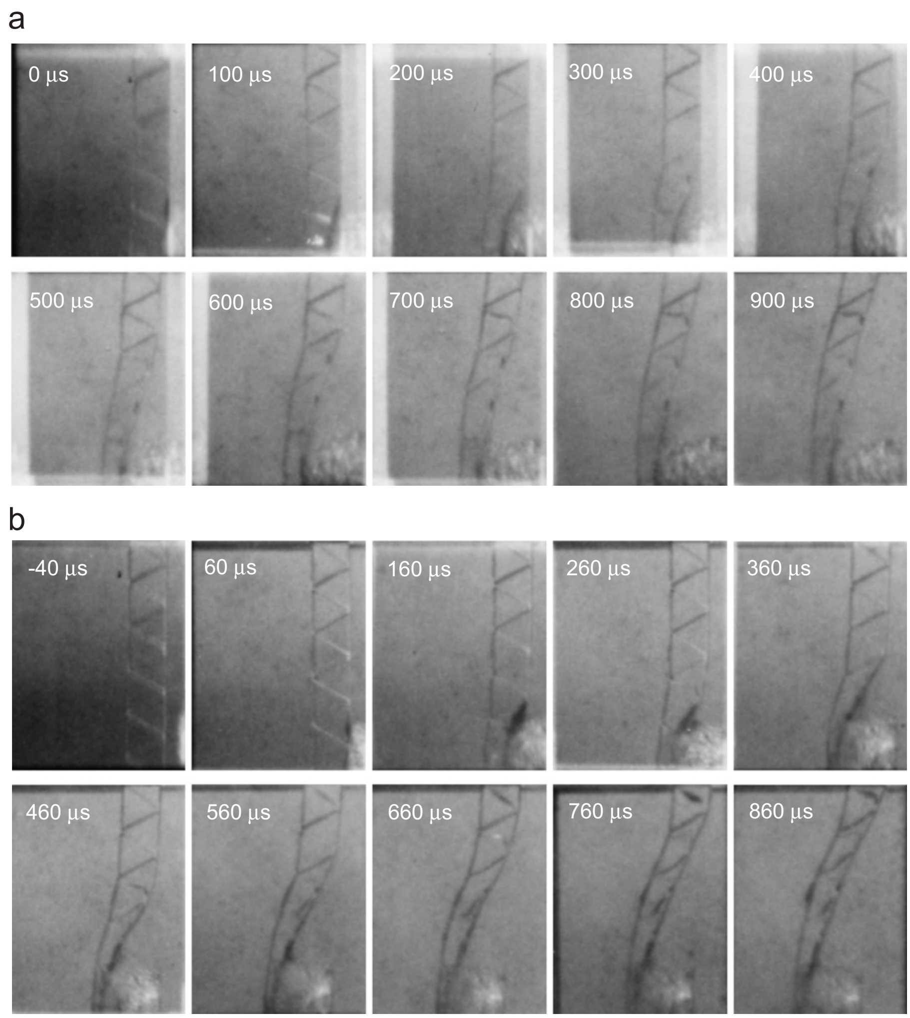


Fig. 14. High-speed photographic sequence of the deformation of the corrugated core sandwich beams (transverse core orientation). (a) $I_0 = 1.5\,\mathrm{kN\,s\,m^{-2}}$ and (b) $I_0 = 2.9\,\mathrm{kN\,s\,m^{-2}}$. The inter-frame time is 100 µs and time $t$ is measured from the instant of the impact.

velocity $v_0$. Thus, the shock width is $w \approx 5\,\mathrm{mm}$ and is of the order observed in shock experiments [18]. Large gradients in stress and strain occur over the shock width and thus the foam projectile was discretised by a mesh size of 1 mm in order to resolve these gradients accurately.

### 4.2. Comparison of finite element predictions and measurements

Sample FE predictions of the maximum mid-span deflection versus time histories of the monolithic and sandwich beams with the longitudinal core arrangement are plotted in Fig. 16 for $I_0 = 3\,\mathrm{kN\,s\,m^{-2}}$. The deflection versus time histories indicate that only small elastic vibrations occur after peak deflection and thus the peak deflection is approximately equal to the final permanent deflection for both the monolithic and sandwich beams.

The predicted mid-span back-face deflections of the monolithic and sandwich beams are included in Figs. 6a and 12 for comparison against the measured values. The permanent deflections in the FE calculations are estimated by averaging the displacements over several cycles of elastic vibration (from trough to peak) immediately after the initial peak displacement. It is concluded that the FE model predicts the permanent deflection accurately for the sandwich beams (longitudinal and transverse core orientations) and for the monolithic beams provided the loading does not induce failure. The failure process is not modelled in the FE calculations and thus the calculations under-predict the deflection for values of $I_0$ above the observed failure threshold. We note that the good agreement between the FE calculations and observations confirms that the clamped boundary conditions assumed in the calculations are representative of the experimental situation. Moreover, it is worth emphasising here that the manufacturing route for the sandwich beams is complicated and invariably introduces manufacturing defects in the beams. While these defects are not explicitly accounted for in the simulations, the good comparisons between the predictions and simulations reveal that these defects do not affect the beam response appreciably.

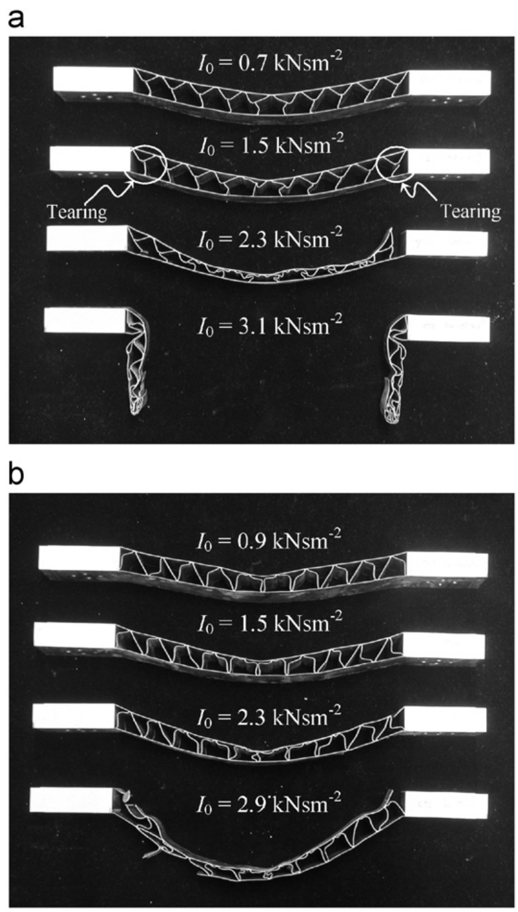


Fig. 15. Photographs showing the deflected profiles of the dynamically loaded (a) Y-frame and (b) corrugated core sandwich beams (transverse core orientation) at selected values of projectile momentum $I_0$.

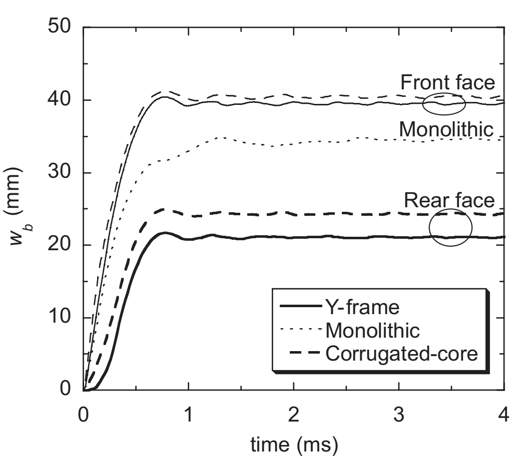


Fig. 16. Finite element prediction of the mid-span deflection versus time histories for monolithic and sandwich beams with (longitudinal core orientation) loaded with a metal foam projectile of $I_0 = 3\,\mathrm{kN\,s\,m^{-2}}$.

The FE predictions of the final core compression $\varepsilon_c$ are included in Fig. 6b for the sandwich beams of longitudinal core orientation. The FE simulations predict the measurements to adequate precision. In order to gauge the ability of the simulations to capture the deformation state of the sandwich cores, the sandwich beams with the longitudinal core arrangement were sectioned at mid-span. A comparison between the observed and FE predictions of the deformed profiles of the Y-frame and corrugated core sandwich beams at mid-span is included in Fig. 17 for the case of $I_0 = 3\,\mathrm{kN\,s\,m^{-2}}$. Reasonable agreement between the observations and predictions is obtained; in particular, the densification of the core due to the contact between the core and face sheets is captured in the simulations.

FE predictions of the progressive deformation of the Y-frame and corrugated core sandwich beams with the transverse core arrangements are included in Figs. 18a and b, respectively, for the choice $I_0 = 1.5\,\mathrm{kN\,s\,m^{-2}}$. Reasonable agreement is obtained between the observations (Figs. 13a and 14a) and predictions including the large degree of core compression beneath the foam projectile and the large shear deformation of the core near the supported ends of the beams. Directly beneath the foam impact site, the corrugated core compresses in a dynamic mode with the deformation concentrated near the front face. In contrast, the deformation of the Y-frame core immediately beneath the foam projectile is similar to its quasi-static deformation mode. This is consistent with observations and FE predictions of Tilbrook et al. [15], which suggest that inertial stabilisation against buckling has a smaller effect upon the bending-dominated Y-frame core than upon the stretching-dominated corrugated core.

### 4.3. Estimation of the onset of failure

The prediction of tearing of beams and plates subjected to shock-type loading has been the object of various numerical studies. These simulations either employ a Johnson–Cook-type failure criterion [16–17,27] or simulate rupture based on a shear strain criterion [28]. These studies suffer from the drawback that including material softening in the FE calculations results in mesh size sensitivity of the

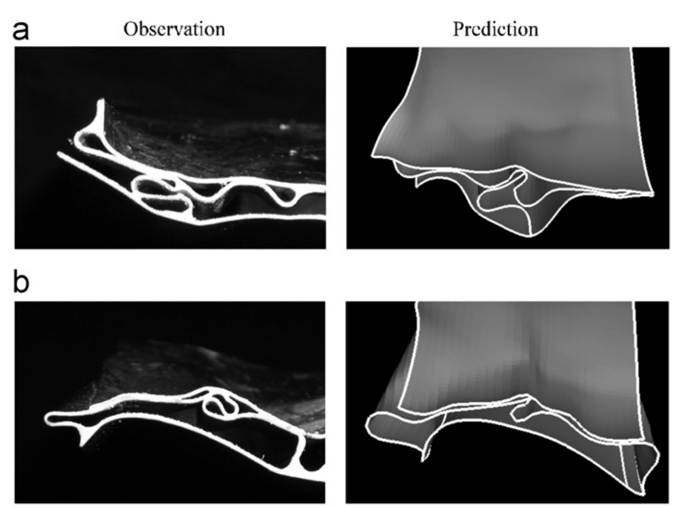


Fig. 17. The mid-span deformed profiles of (a) Y-frame and (b) corrugated core sandwich beams (longitudinal core orientation), for $I_0 = 3\,\mathrm{kN\,s\,m^{-2}}$.

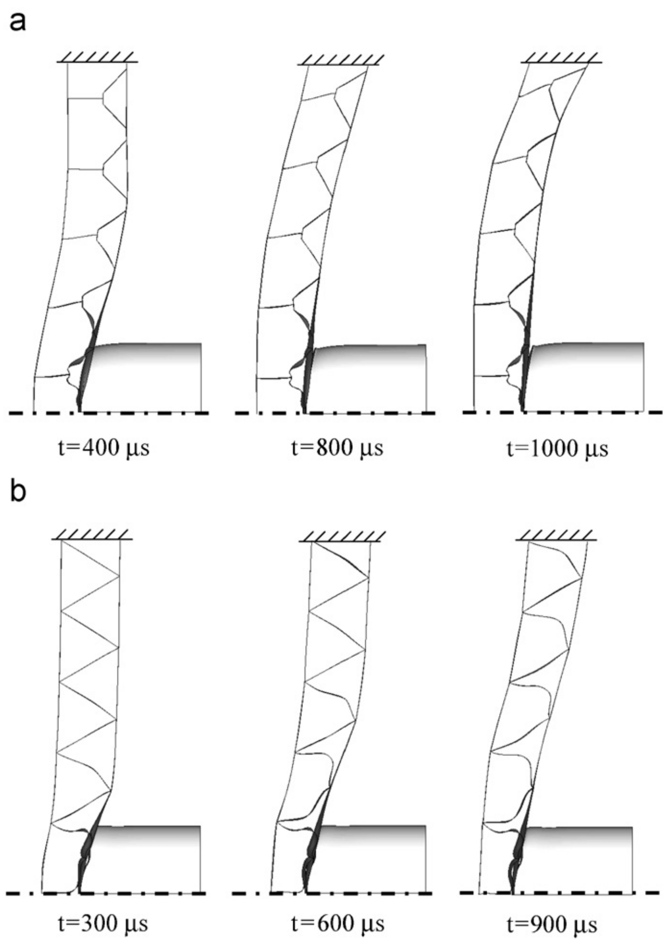


Fig. 18. FE predictions of the time evolution of the deformation of the (a) Y-frame and (b) corrugated core sandwich beams (transverse core orientation) impacted by the foam projectile of $I_0 = 1.5\,\mathrm{kN\,s\,m^{-2}}$. The predictions are shown at three selected times and correspond to the high-speed photographs in Figs. 13a and 14a.

predictions. By contrast, studies such as those by Liang et al. [29] only estimate the onset of tearing using a maximum plastic strain criterion. Here we employ such an approach.

The final plastic strain distribution within the Y-core and corrugated core sandwich beams was explored from the FE simulations for the choice $I_0 = 5.4\,\mathrm{kN\,s\,m^{-2}}$. This impulse level was chosen as it gave failure in the as-brazed Y-core but not in the laser-welded Y-core. The location of maximum principal strain within the sandwich beams of longitudinally arranged Y-frame and corrugated cores are given in Figs. 19a and b, respectively. For both topologies, the maximum strain occurs within the core at $X_1 \approx 25\,\mathrm{mm}$ (i.e. near the edge of the contact between the foam projectile and the beam). For the Y-frame core, the maximum predicted strain occurs at the joint between the leg and web, while for the corrugated core the highest strain occurs at the joint between the core and the front face sheet. The FE simulations predict similar maximum strain levels ($\approx$40%) for both the Y-frame and corrugated core beams, suggesting that the corrugated and Y-frame core beams should fail at similar values of $I_0$. However, the

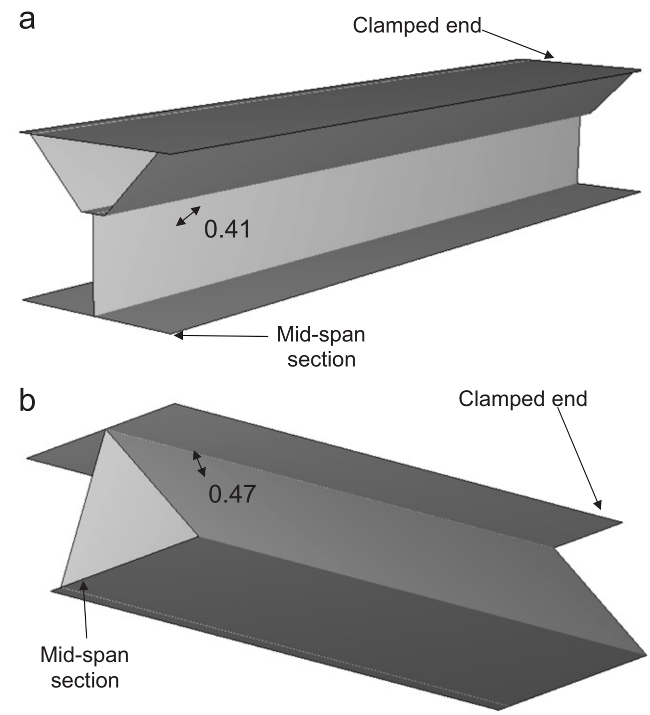


Fig. 19. Sketch representing the FE predictions for the location and direction of the maximum principal strain in the (a) Y-frame and (b) corrugated core sandwich beams (longitudinal core orientation). The beams were impacted by the foam projectile of $I_0 = 5.4\,\mathrm{kN\,s\,m^{-2}}$.

FE model does not include the observed distribution of braze within the joints. The re-entrant corner of the corrugated core draws in more braze than the right-angle joint of the Y-frame and it is thereby locally stronger. This explains the premature failure of the brazed Y-frame beams.

## 5. Concluding remarks

Metal foam projectiles have been used to impact clamped 304 stainless-steel monolithic beams and sandwich beams with Y-frame or corrugated cores. The permanent deflections and level of core compression of the sandwich beams have been measured as a function of projectile momentum, and the measured responses are compared with FE simulations. The FE simulations capture the observed deformation modes to reasonable accuracy including multiple folding of the core at the projectile impact site.

High-speed photographs of the experiments give the time histories of core compression and of the travelling plastic hinges. The sandwich beams with longitudinal core arrangement outperform monolithic beams of equal mass in terms of back face deflections. However, failure in these sandwich beams occurs at lower levels of projectile momentum compared with the equivalent monolithic beams. In contrast, a sandwich beam with a transverse core has a similar rear-face deflection to that of the monolithic beam. Moreover, sandwich beams with a transverse core orientation fail at lower levels of projectile momentum than their monolithic counterparts. It remains to evaluate the performance of a sandwich plate, subjected to dynamic loading at its centre and clamped on its periphery. This is a topic of future study.

## Acknowledgments

This work was supported by the Netherlands Institute for Metal Research: project number MC1.03163, *The Optimal Design of Y-core sandwich structures*.

## References


[1] Wang AJ, Hopkins HG. On the plastic deformation of built-in circular plates under impulsive load. J Mech Phys Solids 1954;3:22–37.

[2] Symonds PS. Large plastic deformation of beams under blast type loading. In: Proceedings of the second US national congress of applied mechanics, 1954. p. 505–15.

[3] Jones N. Impulsive loading of a simply supported circular rigid-plastic plate. J Appl Mech 1968;35:59–65.

[4] Fleck NA, Deshpande VS. The resistance of clamped sandwich beams to shock loading. J Appl Mech 2004;71:386–401.

[5] Xue Z, Hutchinson JW. A comparative study of blast resistant metal sandwich plates. Int J Impact Eng 2004;30:1283–305.

[6] Paik JK. Innovative structural designs of tankers against ship collisions and grounding: a recent state-of-the-art review. Mar Technol 2003;40:25–33.

[7] Wevers LJ, Vredeveldt AW. Full scale ship collision experiments 1998, TNO-report 98-CMC-R1725. The Netherlands, 1999.

[8] Ludolphy H. The unsinkable ship—development of the Y-shape support web. In: Proceedings of the second international conference on collision and grounding of ships. Copenhagen, Denmark, 2001.

[9] Konter A, Broekhuijsen J, Vredeveldt A. A quantitative assessment of the factors contributing to the accuracy of ship collision predictions with the finite element method. In: Proceedings of the third international conference of ship collisions and grounding, Tokyo (Japan), 2004.

[10] Naar H, Kujala P, Simonsen BC, Ludolphy H. Comparison of the crashworthiness of various bottom and side structures. Mar Struct 2002;15:443–60.

[11] Pedersen CBW, Deshpande VS, Fleck NA. Compressive response of the Y-shaped sandwich core. Eur J Mech-A/Solids 2004;25:125–41.

[12] Rubino V, Deshpande VS, Fleck NA. The collapse response of sandwich beams with a Y-frame core subjected to distributed and local loading. Int J Mech Sci 2008;50:233–45.

[13] Rubino V, Deshpande VS, Fleck NA. The three point bending of Y-frame sandwich beams, 2008, in preparation.

[14] Côté F, Deshpande VS, Fleck NA, Evans AG. The compressive and shear responses of corrugated and diamond lattice materials. Int J Solids Struct 2007;43:6220–42.

[15] Tilbrook MT, Radford DD, Deshpande VS, Fleck NA. Dynamic crushing of sandwich panels with prismatic lattice cores. Int J Solids Struct 2007;44:6101–23.

[16] Chung Kim Yuen S, Nurick GN. Experimental and numerical studies on the response of quadrangular stiffened plates. Part I: subjected to uniform blast load. Int J Impact Eng 2005;31:55–83.

[17] Langdon GS, Chung Kim Yuen S, Nurick GN. Experimental and numerical studies on the response of quadrangular stiffened plates. Part II: localised blast loading. Int J Impact Eng 2005;31:85–111.

[18] Radford DD, Fleck NA, Deshpande VS. The use of metal foam projectiles to simulate shock loading on a structure. Int J Impact Eng 2005;31:1152–71.

[19] Radford DD, Fleck NA, Deshpande VS. The response of clamped sandwich beams subjected to shock loading. Int J Impact Eng 2006;32:968–87.

[20] Rathbun HJ, Zok FW, Waltner SA, Mercer C, Evans AG, Queheillalt DT, et al. Structural performance of metallic sandwich beams with hollow truss cores. Acta Mater 2006;54:5509–18.

[21] Deshpande VS, Fleck NA. Isotropic constitutive models for metallic foams. J Mech Phys Solids 2000;48:1253–83.

[22] Stout MG, Follansbee PS. Strain-rate sensitivity, strain hardening, and yield behaviour of 304L stainless steel. Trans ASME: J Eng Mater Technol 1986;108:344–53.

[23] Radford DD, McShane GJ, Deshpande VS, Fleck NA. The response of clamped sandwich plates with metallic foam cores to simulated blast loading. Int J Solids Struct 2006;43:2243–59.

[24] McShane GJ, Radford DD, Deshpande VS, Fleck NA. The response of clamped sandwich plates with lattice cores subjected to shock loading. Eur J Mech-A/Solids 2006;25:215–29.

[25] Côté F, Fleck NA, Deshpande VS. Fatigue performance of sandwich beams with a pyramidal core. Int J Fatigue 2007;29:1402–12.

[26] Ashby MF, Evans AG, Fleck NA, Gibson LJ, Hutchinson JW, Wadley HNG. Metal foams: a design guide. Oxford: Butterworth Heinemann; 2000.

[27] Balden VH, Nurick GN. Numerical simulation of the post-failure motion of steel plates subjected to blast loading. Int J Impact Eng 2005;32:14–34.

[28] Gupta NK, Nagesh. Deformation and tearing of circular plates with varying support conditions under uniform impulsive loads. Int J Impact Eng 2007;34:42–59.

[29] Liang Y, Spuskanyuk AV, Flores SE, Hayhurst DR, Hutchinson JW, McMeeking RM, et al. The response of metallic sandwich panels of water blast. J Appl Mech 2006;74:81–99.